

# Single junction CsPbBr<sub>3</sub> solar cell coupled with electrolyzer for solar water splitting

Received: 10 May 2024

Accepted: 8 April 2025

Published online: 30 July 2025

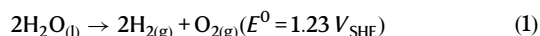
Check for updates

Jin Hyun Kim<sup>1,7</sup> , Jongdeuk Seo<sup>2,7</sup> , Dongjun Lim<sup>2,7</sup> , Jaehwi Lee<sup>2</sup> , Jinhee Kim<sup>2</sup> , Jin Uk Lee<sup>2</sup> , Jong Ah Moon<sup>2</sup> , Jaeki Jeong<sup>1,3</sup> , Shaik Mohammed Zakeeruddin<sup>1</sup> , Heunjeong Lee<sup>4</sup> , Shinuk Cho<sup>4</sup> , Michael Graetzel<sup>1</sup> , Hankwon Lim<sup>2,5,6</sup> , Jae Sung Lee<sup>2</sup> & Jin Young Kim<sup>2,6</sup>

Artificial photosynthesis system to realize Solar overall water splitting has been regarded as sustainable and renewable solution for energy and environmental issues. While artificial photosynthesis system (efficiency of 12.4%) greatly exceeds efficiency of natural photosynthesis, yet such high efficiency needs multiple, 2 or more light absorbers to achieve, total photovoltage above 1440 mV. In this report, we demonstrate visible light active Single light absorber – 2 photons to 1 hydrogen (S2) overall water splitting via photovoltaic–electrochemical system that can be achieved by single junction solar cell, composed with CsPbBr<sub>3</sub> (band gap of 2.3 eV) solar cell with open circuit voltage larger than 1600 mV can power up water electrolyzer cell and achieves Solar to hydrogen efficiency of 1.7% with confirmed H<sub>2</sub> gas generation. Operating point shows possible STH of 5.0%. This result demonstrates its prospective on efficiency increment (max 12%) and Technoeconomic analysis (modest cost of 5.5 \$/kg of hydrogen) in near future, as benchmark for S2 PV-EC system.

Solar overall water spitting (SOW) has been regarded as an ideal way to harvest and store solar energy into clean and CO<sub>2</sub> neutral reaction<sup>1–3</sup>. Overall water splitting can be described as simple formula.

Overall water-splitting reaction:



Including overpotential for reaction, which is ~200 mV for oxygen evolution reaction (OER) and ~15 mV for hydrogen evolution reaction (HER) @ 2 mA cm<sup>-2</sup> (current density that can be presumed to generate O<sub>2</sub> and H<sub>2</sub> with agreeable Faradaic efficiency (FE)) if state of art electrocatalysts are used<sup>4</sup>, overall water splitting takes more than 1440 mV

to conduct (onset potential wise, 200 mV for Ir and 10 mV for Pt)<sup>4</sup>, if electrolysis approach is taken. Regardless of the systems used for SOW, this requirement is commonly applied that light absorber(s) must achieve photovoltage ( $V_{\text{ph}}$ ) above 1440 mV to conduct the reaction. Solar-to-hydrogen efficiency ( $\eta_{\text{STH}}$ ) can be described by below formula<sup>5</sup>

$$\eta_{\text{STH}} = \left[ \frac{J_{\text{SC}} \times (1.23) \times \eta_{\text{F}}}{P_{\text{Total}}} \right]_{\text{AMI.5G}} \quad (2)$$

where  $J_{\text{SC}}$  is the short-circuit photocurrent density (mA cm<sup>-2</sup>) or rate of H<sub>2</sub> production converted to a current density,  $\eta_{\text{F}}$  is the Faradaic

<sup>1</sup>Laboratory of Photonics and Interfaces, Institute of Chemical Sciences and Engineering, School of Basic Sciences, Ecole Polytechnique Fédérale de Lausanne (EPFL), CH-1015 Lausanne, Switzerland. <sup>2</sup>School of Energy and Chemical Engineering, Ulsan National Institute of Science & Technology (UNIST), Ulsan 44919, Republic of Korea. <sup>3</sup>Department of Energy Science, Sungkyunkwan University, Suwon 16419, Republic of Korea. <sup>4</sup>Department of Physics and Energy Harvest Storage Research Center (EHSRC), University of Ulsan, Ulsan 44610, Republic of Korea. <sup>5</sup>Carbon Neutrality Demonstration and Research Center, Ulsan National Institute of Science and Technology (UNIST), Ulsan 44919, Republic of Korea. <sup>6</sup>Graduate School of Carbon Neutrality, Ulsan National Institute of Science & Technology (UNIST), Ulsan 44919, Republic of Korea. <sup>7</sup>These authors contributed equally: Jin Hyun Kim, Jongdeuk Seo, Dongjun Lim.

e-mail: [jinhyun.kim@epfl.ch](mailto:jinhyun.kim@epfl.ch); [hklim@unist.ac.kr](mailto:hklim@unist.ac.kr); [jlee1234@unist.ac.kr](mailto:jlee1234@unist.ac.kr); [jykim@unist.ac.kr](mailto:jykim@unist.ac.kr)

efficiency of  $\text{H}_2$  production (usually ~100%), and  $P_{\text{Total}}$  is the solar incident irradiance intensity ( $100 \text{ mW cm}^{-2}$  for air mass (AM) 1.5 G).

To achieve SOW, various strategies are taken into consideration, for 5 decades of research effort have been invested for photocatalysis (PC,  $\eta_{\text{STH}}$  0.65%  $\text{Al:SrTiO}_3$ <sup>6</sup> for S2 and 1.2% for  $\text{BiVO}_4/\text{Rh:SrTiO}_3$ <sup>7</sup>), photoelectrochemical (PEC,  $\eta_{\text{STH}}$  3.0%  $\text{BiVO}_4/\text{Cu}_2\text{O}$ <sup>7</sup>, 6.2%  $\text{BiVO}_4/\text{PSC}$ <sup>8</sup>, 19%  $\text{GaInP/GaInAs}$ <sup>9</sup>) and photovoltaic–electrochemical system (PV-EC, 30% for triple junction  $n$  III–V–2 PEM<sup>10</sup>, 20% for PSC/Si<sup>11</sup>), the spectrum of approach has been widened which depends on what type of light absorber is used. Thus, the role of the light absorber is the most important for realizing SOW, while water electrolysis (with various cell types) is a more established technology with a wide choice of materials (noble metals represented by Ir, Ru, and Pt, transition metal–N/P/S and Se etcetera)<sup>12,13</sup>.

As noted above, it is seldom achieved that single light absorber–2 photons to 1 hydrogen (co called S2, theoretical  $\eta_{\text{STH}}$  ~12%) based system and the state of art efficiency is rather low (0.65%). In the meantime, dual light absorbers–4 photons to 1 hydrogen (D4, theoretical  $\eta_{\text{STH}}$  ~24%) and even triple light absorbers–6 photons to 1 hydrogen (T6, theoretical  $\eta_{\text{STH}}$  ~20%) are rather commonly reported and efficiency, as marked above, is well established, from 10% to 20% for PV-EC depending on PV used for the system<sup>14,15</sup>. As marked and demonstrated by Sayama and Miseki<sup>16–18</sup>, the realization of different systems besides highly efficient D4 overall water splitting, but diversifying light utilization system (number of light absorbers) and sorts of redox reaction (such as  $\text{H}_2\text{O}_2$ , which has very different energy requirement and reaction kinetics than overall water splitting), can perhaps hasten the realization of feasible solar fuel production.

Technoeconomic analysis (TEA) of SOW with various materials and scenarios<sup>5,19,20</sup> showed that there are three major factors—(1) life span of system (>10 years), (2)  $\eta_{\text{STH}}$  (5–20% for different systems) and (3) cost of the entire system that is involved in the production of hydrogen, the so-called leveled cost of hydrogen (LCOH) which is the major metric for SOW for commercialization. While a life span of 10 years has never been achieved, what has been regarded factor was  $\eta_{\text{STH}}$ /cost of device balance that expensive light absorbers present high  $\eta_{\text{STH}}$  but with poor LCOH value (above 10\$/kg). The analysis showed that LCOH with feasible value often comes out from a system using multijunction light absorbers<sup>5,21,22</sup>.

While in multijunction, even though the light absorber component was one,  $\eta_{\text{STH}}$  of 3.4% was achieved by using an expensive III–V  $\text{InGaP}$  photocathode<sup>23</sup>, which is the only one report using S2 system with efficiency above 1.0% to the best of our knowledge, plus with visible light activity. Despite this demonstration, a true single  $n$ – $i$ – $p$  junction to conduct S2 OWS was never achieved with efficiency above 1.0%.

The key may lay on recent innovation made for lead halide perovskite light absorbers with a combination of cation/Pb/halogen anions have shown drastic improvement in performance, achieving 26.5% PCE with open-circuit voltage ( $V_{\text{OC}}$ , same as  $V_{\text{ph}}$ ) of 1192 mV<sup>24</sup>. Indeed, SOW could be achieved by lead halide perovskite solar cell (PSC), a pioneering work presented by Luo et al. to show 2 series connected  $\text{MAPbI}_3$  ( $\eta_{\text{STH}}$  12.3%)<sup>25</sup>, followed by realizing 2jn PSC/Si ( $\eta_{\text{STH}}$  19%)<sup>26</sup> and the most elegant and effective 2jn PSC ( $\eta_{\text{STH}}$  13.1%)<sup>27</sup> was demonstrated. (discussion made in Supplementary Fig. 2).

On top of such high efficiency, one of the biggest strengths of lead halide perovskite for solar energy conversion and especially for solar fuel generation is band gap tunability by controlling the composition of the anion (Cl/Br/I) that subsequently enlarges band gap from  $\text{MAPbI}_3$  (1.5 eV), if more Br or Cl ratio is increased, thus  $V_{\text{ph}}$  achievable from PSC is increased from 1100 mV to larger value. For solar cells with a single light absorber, the ideal band gap is 1.3–1.4 eV<sup>28</sup>. As the band gap of the light absorber increases over 1.4 eV by compositional engineering<sup>29</sup> the solar cell can only absorb a shorter wavelength of visible light, which leads drop in photocurrent. Despite this severe loss

of photocurrent, wide band gap PSCs are still worth studying, due to their higher  $V_{\text{OC}}$ . As summarized in Supplementary Fig. 1 and Supplementary Table 1, the narrower band gap perovskites show high efficiency but low  $V_{\text{OC}}$ , while the wide band gap perovskites exhibit higher  $V_{\text{OC}}$  due to the capability of absorbing high photon energy. There is a very interesting one which is wide band gap perovskite light absorbers, one represented by  $\text{MAPbBr}_3$  and  $\text{CsPbBr}_3$  could achieve above 1600 mV and PCE above 10% for both  $n$ – $i$ – $p$  and  $p$ – $i$ – $n$  structure, which is unrepresentedly high  $V_{\text{OC}}$  for PV devices<sup>30</sup>.

In this report, we demonstrated a single junction solar cell powered PV-EC SOW, with a modest  $\eta_{\text{STH}}$  of 1.7% for confirmed  $\text{H}_2/\text{O}_2$  gas evolution for 3 h of stability, even for monolithic cells working immersed in water. Technological difference between previously reported Halide perovskite light absorber-based solar water splitting (end product: hydrogen) was described in Supplementary Figs. 2, 3. Following analysis such as theoretical  $\eta_{\text{STH}}$  of ~12% reachable by using  $\text{CsPbBr}_3$  (2.2–2.3 eV) and modest value of LCOH of 5.5\$/kg also support that our demonstration should present a promising scenario for SOW technology.

## Results

### $\text{CsPbBr}_3$ perovskite solar cells

For PSC to provide electrical power in PV-EC system, we chose all-inorganic  $\text{CsPbBr}_3$  instead of  $\text{MAPbBr}_3$ , because  $\text{MAPbBr}_3$  is well-known for its inferior stability owing to its unstable methylammonium cation<sup>31</sup>. Prior to the test of the whole PV-EC system, a brief analysis of only PSCs was carried out with the device structure of  $\text{FTO}/\text{c-TiO}_2/\text{SnO}_2/\text{CsPbBr}_3/\text{PTAA}/\text{MoO}_3/\text{Au}$  (Fig. 1a). In Fig. 1b, the cross-sectional scanning electron microscopy (SEM) image represents sequential deposition of the  $\text{CsPbBr}_3$  PSC. Based on the fact that metal carbonate salts can enhance the performance of the PSC by adjusting band alignment, we tested  $\text{Li}_2\text{CO}_3$  on the  $\text{TiO}_2/\text{SnO}_2$  electron transport layer (ETL) to achieve sufficient  $V_{\text{OC}}$ <sup>32</sup>. We referred to a study performed by J.Y. Kim et al., which demonstrated that metal carbonate salts can enhance the performance of the PSC by adjusting band alignment<sup>33</sup>. To achieve sufficient  $V_{\text{OC}}$ , we tested  $\text{Li}_2\text{CO}_3$  on the  $\text{TiO}_2/\text{SnO}_2$  electron transport layer (ETL) and the corresponding energy diagram of the PSCs was depicted in Fig. 1c. The conduction band minima (CBM) and the valence band maxima (VBM) of ETL and  $\text{CsPbBr}_3$  films were calculated from the ultraviolet photoelectron spectroscopy (UPS) measurements (Supplementary Figs. 4–7). We predicted the  $V_{\text{OC}}$  loss of PSC with  $\text{Li}_2\text{CO}_3$  treatment shown to be reduced since the CBM of  $\text{SnO}_2$  gets closer to that of  $\text{CsPbBr}_3$  after the treatment. The device performances are shown in Fig. 1d, e and Supplementary Table 2. The PSCs with  $\text{Li}_2\text{CO}_3$  treatment exhibited a higher  $V_{\text{OC}}$  of 1.50 V than the pristine one with a  $V_{\text{OC}}$  of 1.37 V, while both devices show the almost same PCE. Although we achieved a champion  $V_{\text{OC}}$  of 1.63 V during device optimization (Supplementary Fig. 8), the corresponding device exhibited poor  $J_{\text{SC}}$ , leading us to exclude it from the following experiments.

For deeper investigation of this phenomenon, transient photovoltage (TPV) and transient photocurrent (TPC) measurement for the devices (Supplementary Fig. 9). The increase of photovoltage decay time from 4.393 to 6.335  $\mu\text{s}$  after  $\text{Li}_2\text{CO}_3$  treatment indicates the reduction of recombination rate, due to the elimination of oxygen vacancies of  $\text{SnO}_2$  and reduced charge accumulation by band rearrangement, which is consistent with  $V_{\text{OC}}$  improvement. Photoluminescence measurement of  $\text{CsPbBr}_3$  film showed increased PL intensity for the  $\text{Li}_2\text{CO}_3$  treated film, which indicates reduced recombination of photocarriers (Supplementary Fig. 10). Meanwhile, the increased decay time of photocurrent from 0.8405 to 1.317  $\mu\text{s}$  after  $\text{Li}_2\text{CO}_3$  treatment indicates hindered charge extraction by the insulating  $\text{Li}_2\text{CO}_3$  layer which gives rise to low short-circuit current density in operating conditions. We further tested other types of alkali metal carbonates ( $\text{Na}_2\text{CO}_3$ ,  $\text{K}_2\text{CO}_3$ ,  $\text{Rb}_2\text{CO}_3$ , and  $\text{Cs}_2\text{CO}_3$ ), but none of them showed higher  $V_{\text{OC}}$  than the one treated with  $\text{Li}_2\text{CO}_3$  (Supplementary

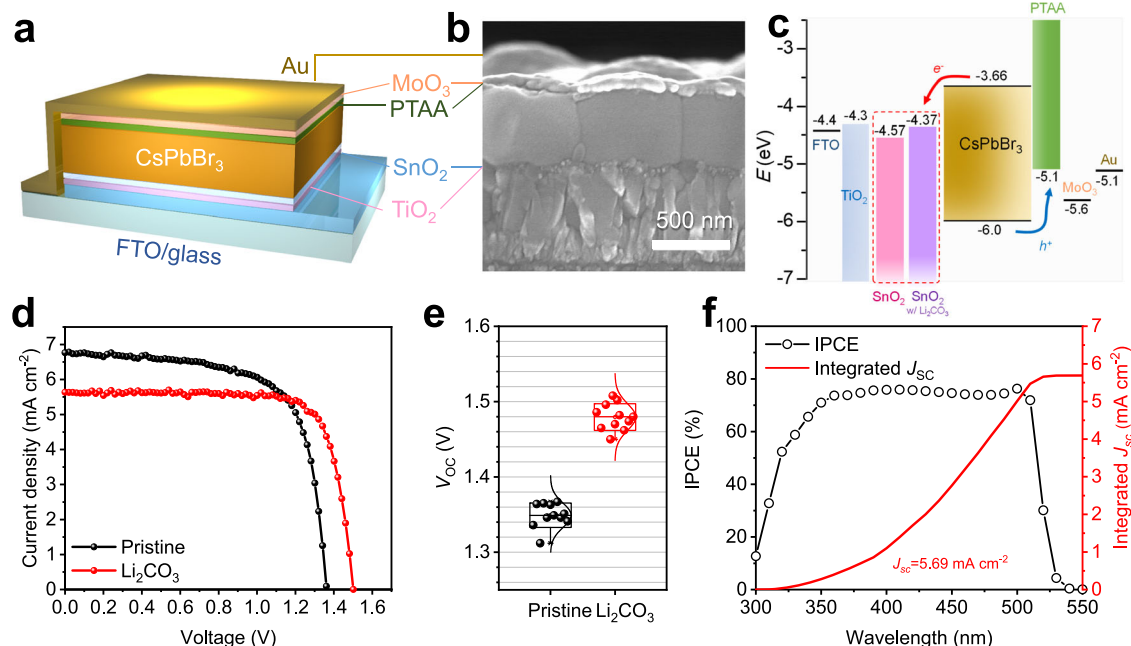


**Fig. 1 | Characteristics of the CsPbBr<sub>3</sub> PSCs.** **a** Configuration, **b** cross-sectional SEM image and **c** energy diagram of the CsPbBr<sub>3</sub> PSCs. **d** Performance comparison and **e**  $V_{OC}$  distribution of the CsPbBr<sub>3</sub> PSCs without (black sphere) and with (red

sphere) Li<sub>2</sub>CO<sub>3</sub> treatment. **f** IPCE measurement (black circle) and integrated  $J_{SC}$  (red line) of the Li<sub>2</sub>CO<sub>3</sub> treated CsPbBr<sub>3</sub> PSC.

Fig. 11). The Mott-Schottky plot reveals the highest built-in voltage of the Li<sub>2</sub>CO<sub>3</sub> treated device, in agreement with the UPS measurements (Supplementary Fig. 12). Considering overpotential required in PV-EC configuration, solar cells with higher  $V_{OC}$  are preferred, for which Li<sub>2</sub>CO<sub>3</sub> was used in our every following experiment. The operating prediction in Supplementary Fig. 13 shows the advantage of a higher  $V_{OC}$  over a higher  $J_{SC}$ . In Fig. 1f, incident photon to current efficiency (IPCE) measurement for the Li<sub>2</sub>CO<sub>3</sub> treated solar cell showed a calculated  $J_{SC}$  of 5.69 mA cm<sup>-2</sup>, which verifies the  $J_{SC}$  obtained from the  $J$ - $V$  curve not to be overvalued. The  $V_{OC}$  of Li<sub>2</sub>CO<sub>3</sub> treated PSC exceeds the minimum value of 1.44 V required in the overall water-splitting reaction, which satisfies the condition to electrolyze H<sub>2</sub>O into O<sub>2</sub> and H<sub>2</sub> with this single-junction solar cell. Please note that the  $V_{OC}$  of our device is not the highest level, but a comparable value with recently reported results (Supplementary Fig. 14, Supplementary Tables 3, 4).

We also fabricated a MAPbBr<sub>3</sub> PSC to compare with a CsPbBr<sub>3</sub> PSC. The performance of the MAPbBr<sub>3</sub> PSC and CsPbBr<sub>3</sub> PSC is shown in Supplementary Fig. 15. In our case, the MAPbBr<sub>3</sub> PSC had an inadequate  $V_{OC}$  of 1.40 V for SOW even though it exhibited a much higher  $J_{SC}$  of 7.04 mA cm<sup>-2</sup> than the CsPbBr<sub>3</sub> PSC with  $J_{SC}$  of 5.63 mA cm<sup>-2</sup>. Photostability for both PSCs was measured under 1 sun irradiation in ambient air without encapsulation (Supplementary Fig. 16). As expected, the MAPbBr<sub>3</sub> PSC underwent fast degradation of PCE. On the other hand, the CsPbBr<sub>3</sub> PSC maintained more than 70% of initial PCE after 150 h, suggesting that CsPbBr<sub>3</sub> perovskite is suitable for water splitting system rather than MAPbBr<sub>3</sub> perovskite.

### Single junction PV-EC with CsPbBr<sub>3</sub> perovskite solar cell

To realize PV-EC system, EC was composed of an anode and cathode for water oxidation and reduction. For the anode, IrO<sub>x</sub>/Ti foil, NiFeO<sub>x</sub>/Ni foil, or NiFeO<sub>x</sub>/Ni foam were used while for the cathode, Pt/Ti foil, Pt/Ni foil or Pt/Ni foam were used. Basic characterization was done for those materials to confirm the morphology and chemical state of that catalyst on various substrates (Supplementary Figs. 17–19 for SEM, Supplementary Fig. 20 for XRD, and Supplementary Figs. 21–23 for XPS).  $I$ - $V$  curve of a combination of IrO<sub>x</sub>/Ti–Pt/Ti and NiFeO<sub>x</sub>/Ni + Pt/Ni foil or foam showed that both combinations could achieve overall

water splitting with current density over 1.0 mA/cm<sup>2</sup> @ 1.50 V versus counter electrode (CE) with two electrode configuration (Supplementary Fig. 24), thus powering this electrolyzer can be possible with solar cell with  $V_{OC}$  over 1500–1600 mV. Figure 2a shows the schematic and energetic configuration of a single light absorber–2 photons for 1 hydrogen molecule PV-EC system. The performance of CsPbBr<sub>3</sub> PSC with an active area of 0.135 cm<sup>2</sup> showed  $V_{OC}$  of 1550 mV and PCE of 6.5%, which agrees with the one tested as a PV device only. This  $V_{OC}$  was enough to power up alkaline EC whose onset potential in two electrode modes was 1.47 V (IrO<sub>x</sub>/Ti–Pt/Ti), 1.42 V (NiFeO<sub>x</sub>/Ni foil–Pt/Ni foil), 1.40 V (NiFeO<sub>x</sub>/Ni foam–Pt/Ni foam), versus counter electrode (Fig. 2b). Operating point of CsPbBr<sub>3</sub> PV with three different EC was 1.63 mA/cm<sup>2</sup> (IrO<sub>x</sub>/Ti–Pt/Ti), 3.50 mA/cm<sup>2</sup> (NiFeO<sub>x</sub>/Ni foil–Pt/Ni foil), 4.07 mA/cm<sup>2</sup> (NiFeO<sub>x</sub>/Ni foam–Pt/Ni foam). This value can be calculated to  $\eta_{STH}$  of 2.0%, 4.3%, and 5.0%.

More accurate performance can be measured by  $I$ - $V$  curve of CsPbBr<sub>3</sub> PV connected to electrolyzers, (Fig. 2c, b, d) 2.0 mA/cm<sup>2</sup> (IrO<sub>x</sub>/Ti–Pt/Ti), 2.5 mA/cm<sup>2</sup> (NiFeO<sub>x</sub>/Ni foil–Pt/Ni foil), 2.74 mA/cm<sup>2</sup> (NiFeO<sub>x</sub>/Ni foam–Pt/Ni foam). This value can be calculated to  $\eta_{STH}$  of 2.0%, 3.0% and 3.4% for alkaline EC if FE is 100% for hydrogen production.

To confirm the effectiveness of CsPbBr<sub>3</sub> PSC for SOW system, we also measured two electrode response of IrO<sub>x</sub>/Ti–CsPbBr<sub>3</sub> PV connected as working electrode, so voltage saving by CsPbBr<sub>3</sub> PSC can be directly reflected to electrochemical cell. Since highly porous electrode such as Ni foam can present a lot of capacitive current (Supplementary Figs. 25–28)<sup>24</sup>. During measurement of PV-EC, CsPbBr<sub>3</sub> PV showed slight degradation of  $V_{OC}$  of 50 mV (Supplementary Fig. 29), short term stability could be achieved for the most active combination of PV-EC (Supplementary Fig. 30), we intentionally picked IrO<sub>x</sub>/Ti and Pt/Ti as standard data, observation and discussion about this can be found in supplementary information. In Fig. 2c, IrO<sub>x</sub>/Ti WE showed onset at 1.41 V versus CE, while IrO<sub>x</sub>/Ti–CsPbBr<sub>3</sub> PV WE showed onset potential at –0.11 V versus CE, which is 1520 mV shift of onset potential. If current density of 2.0 mA/cm<sup>2</sup> generated at 0.0 versus CE for PV-EC system does not contain capacitance current which does not contribute to O<sub>2</sub> and H<sub>2</sub> production, it is safe to conclude that current density at 0.0 V versus CE results  $\eta_{STH}$  value of 1.7%. Such discrepancy

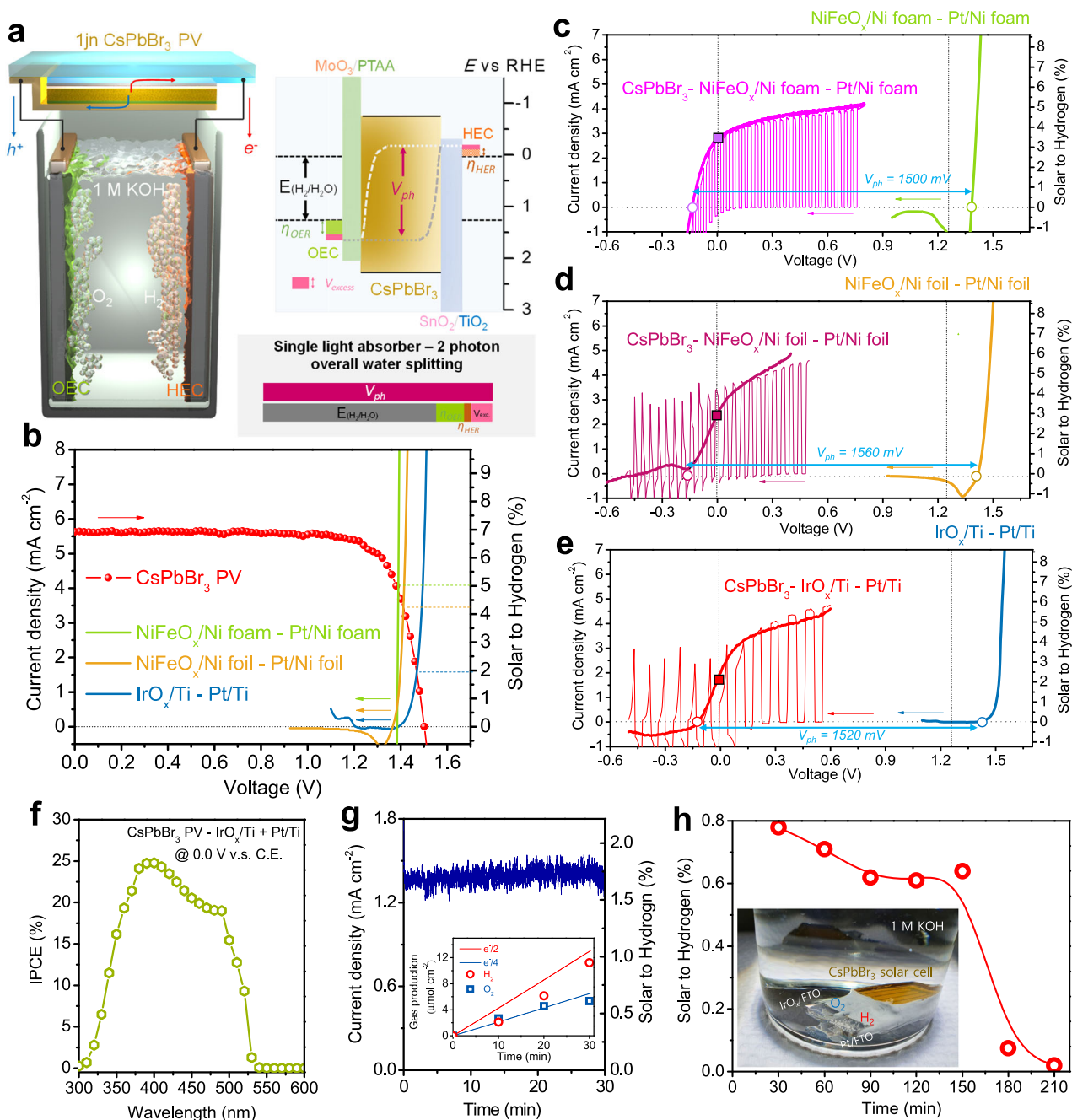


**Fig. 2 | Single light absorber–1 photon electron overall water splitting (S2) via single junction (1jn) CsPbBr<sub>3</sub> PV–alkaline electrolyzer. a** Schematic, **b** operating point prediction of PV and EC, **I/V** curve in two electrode configuration–working electrode with or without PV and counter electrode: **c** working electrode: NiFeO<sub>x</sub>/Ni foam, counter electrode: Pt/Ni foam, **d** working electrode: NiFeO<sub>x</sub>/Ni foil, counter electrode: Pt/Ni foil, **e** working electrode: IrO<sub>x</sub>/Ti, counter electrode: Pt/Ti. PV photoactive area 0.135 cm<sup>2</sup>, electrocatalyst: 1.0 cm<sup>2</sup> for anode and cathode each. Scan

speed for electrocatalyst: **c** 1 mV/s, **d** 20 mV/s and **e** 10 mV/s each. PV-EC was measured with 20 mV/s. **f** IPCE of CsPbBr<sub>3</sub>–IrO<sub>x</sub>/Ti as working electrode (WE) for two electrode configurations under 0.0 V vs. Pt/Ti counter electrode (CE). **g** current response under chopped light with 0.0 V versus counter electrode, the inset figure is for the constant potential of 0.0 V versus counter electrode and gas evolution. **h** Inset picture is for monolithic device working inside of electrolyte and  $\eta_{\text{STH}}$  calculated by evolved gas (only H<sub>2</sub> accounted). **I/V** curves in this figure set are not *iR* corrected.

of  $\eta_{\text{STH}}$  red from operating point (2.4%) to gas evolution of 1.7% is quite often observed for realization of full system instead of expectation from individual components measured separately, as well as small current density generated from system (light absorber was only 0.135 cm<sup>2</sup> big) was rather small to saturate inner space of reactor for gas evolution evaluated by GC<sup>34,35</sup>. Photon wavelength dependent response of CsPbBr<sub>3</sub>–EC till 530 nm was confirmed by IPCE at 0.0 V vs. CE (Fig. 2f). H<sub>2</sub> and O<sub>2</sub> gas evolution was tested for short term and it showed modest ~90% FE at 30 min of operation, which means most of current contributes to H<sub>2</sub> generation (Fig. 2g).

Finally, monolithic device of IrO<sub>x</sub>/FTO–CsPbBr<sub>3</sub> PV–Pt/FTO with epoxy encapsulation could be made, based on its modest ambient and in-water stability as PV (Supplementary Fig. 24). Such functionality will aid to fulfill integrated geometry of PV–EC device to realize monolithic artificial leaf, as demonstrated in Fig. 2h. The device generated H<sub>2</sub> and O<sub>2</sub> bubble spontaneously as it was illuminated under simulated sun or real sun (~0.5 sun intensity), with  $\eta_{\text{STH}}$  of ~0.8% (if active area is set to 0.135 × 4 = 0.54 cm<sup>2</sup>) at beginning but sudden drop at ~180 min, indicating that the stability was jeopardized not because of CsPbBr<sub>3</sub>'s inherent instability but imperfect encapsulation (Supplementary



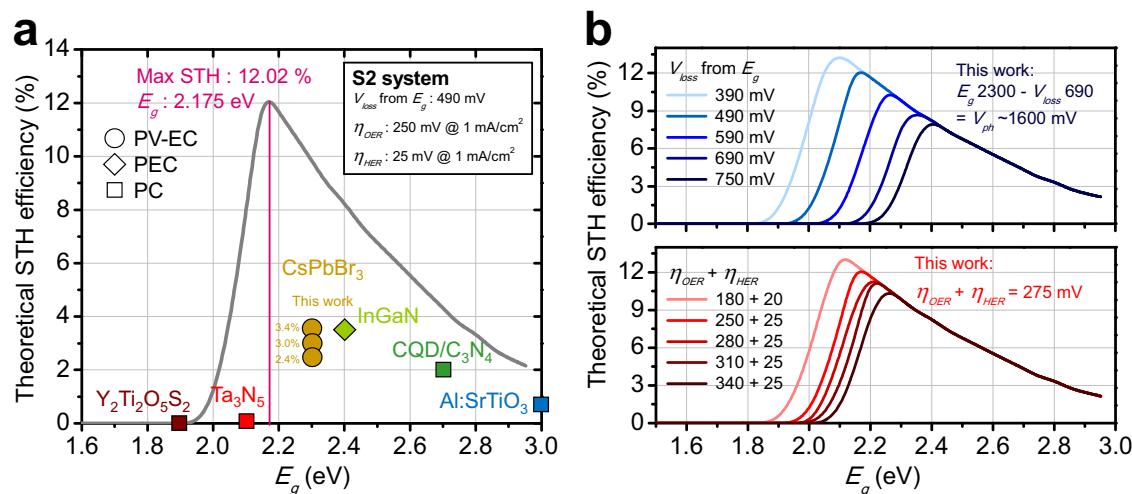


**Fig. 3 | Theoretical  $\eta_{STH}$  achievable from S2 system and relevant parameters.**

**a**  $\eta_{STH}$  of S2 overall water splitting technology in comparison, theoretical  $\eta_{STH}$  calculated with various **b**  $V_{loss}$  in relation to  $E_g$  and  $\eta_{EC}$  of electrolyzer cell. Calculation was conducted by using simulation software provided by Seger et al.<sup>38</sup>. PV efficiency was simulated with the assumption that EQE of the cell can reach 100%, max  $V_{OC}$  will be limited by SQ limit (~490 mV in relation to  $E_g$  of light absorber for PV), with a maximum Fill factor of PV to be 80.0%. Exemplary input is shown in

Supplementary Fig. 32. Reported single light absorber–2 photons for overall water splitting systems from ref. 6 (Al:SiTiO<sub>3</sub>–RhCrO<sub>x</sub> + CoO<sub>x</sub>,  $\eta_{STH}$  0.65 %), ref. 49 (CdTe/C<sub>3</sub>N<sub>4</sub>,  $\eta_{STH}$  2.0 %), ref. 23 (InGa<sub>0.9</sub>N<sub>0.1</sub>–Pt + IrO<sub>x</sub>,  $\eta_{STH}$  3.4%), ref. 50. (Ta<sub>3</sub>N<sub>5</sub>/NaTaO<sub>3</sub>–RhCrO<sub>x</sub> + IrO<sub>x</sub>,  $\eta_{STH}$  0.014%), ref. 51 (Y<sub>2</sub>Ti<sub>2</sub>O<sub>5</sub>S<sub>2</sub>–RhCrO<sub>x</sub> + IrO<sub>x</sub>,  $\eta_{STH}$  0.007%), this work (SnO<sub>2</sub>/CsPbBr<sub>3</sub>/PTAA–IrO<sub>x</sub>/Ti + Pt/Ti,  $\eta_{STH}$  2.4%) (NiFeO<sub>x</sub> and Pt on Ni foil,  $\eta_{STH}$  3.0%) (NiFeO<sub>x</sub> and Pt on Ni foam,  $\eta_{STH}$  3.4%). All referred reports demonstrated quantified gas evolution of hydrogen and oxygen.

Fig. 31). Since activity of IrO<sub>x</sub>/FTO and Pt/FTO were a lot lower than NiFeO<sub>x</sub>/Ni and Pt/Ni, replacing them and optimizing module will increase this value significantly.

Prospective of such device-wide band gap PSC for S2 water splitting is bright and higher efficiency is readily achievable. Considering the reported state-of-the-art CsPbBr<sub>3</sub> solar cell achieved PCE of 10%,  $J_{SC}$  of and  $V_{OC}$  of 1600 mV<sup>36</sup>, even though it is not tested in this report, usage of their PV cell can achieve a lot higher  $\eta_{STH}$  of 8%. If CsPbBr<sub>3</sub> PV achieves its near maximum efficiency of PCE 12% and  $V_{OC}$  of 1.7 V, expectable  $\eta_{STH}$  is 11.5% which is above the value frequently addressed to be criteria for practical solar hydrogen production. It is also near the maximum  $\eta_{STH}$  achievable by the S2 system, calculated by Jaramillo et al.<sup>5</sup> and Atwater et al.<sup>37</sup>.

### Techno-economic analysis for solar hydrogen production via CsPbBr<sub>3</sub>-EC

Before conducting techno-economic analysis (TEA), we made a simple expectation of our device, 1jn CsPbBr<sub>3</sub>-Alkaline EC cell in terms of expected PV's and EC's efficiency (Fig. 3) by using a simple program provided and demonstrated by Seger et al.<sup>38</sup>. Two major governing factors—(1)  $V_{OC}$  for PV and (2) overpotential for EC ( $\eta_{EC}$ ) cell were picked to simulate S2 system showed that our report's parameters—for CsPbBr<sub>3</sub> PV,  $V_{OC}$  loss ~590 mV and for EC cell, overpotential for OER (250 mV) + HER (25 mV) with 30 and 15 mV/dec each (resistance between electrode caused by membrane is ignored since current range for operation is small, 2–5 mA/cm<sup>2</sup>), with assumption that IPCE (50% → 100%) and fill factor (FF) (65% → 80%) can be improved,  $\eta_{STH}$  can reach 12%. Obviously, the major drawback was the performance of CsPbBr<sub>3</sub>, which can be improved in the near future in terms of IPCE and FF. Also, since Halide perovskite light absorbers are easily band gap tunable, a slight reduction of band gap from 2.3 to 2.2 eV will meet the requirement for maximum  $\eta_{STH}$  of 12% easily, thus it is safe to set two parameters for TEA—(1) base case  $\eta_{STH}$  of 8 % (readily achievable in lab scale, considering efficiency reported from other literature, Supplementary Table 3) and (2) maximum reachable  $\eta_{STH}$  of 12%.

Theoretical maximum of S2 ( $\eta_{STH}$  of 12%) is obviously much lower than that of D4 ( $\eta_{STH}$  of 24–28%)<sup>5,37</sup>. Yet, the S2 OWS system uses less cost for light absorber and device since 1jn is needed rather than 2jn.

Since light absorber and power generator (=solar panel for PV-EC) take the majority of cost and energy consumption (40–70%)<sup>39</sup>, S2 has an advantage in reducing capital cost for SOW. Therefore, we conducted a techno-economic analysis for S2 OWS via PV-EC, to see the possibility and potential of S2 OWS in comparison to well-known D4 OWS.

Based on the techno-economic model, the LCOH for the base case is calculated to be 8.4\$/kg (Fig. 4b), with the assumption that  $\eta_{STH}$  reaches 8.0% (Supplementary Table 6). The result indicates that electrocatalyst accounts for the largest portion followed by soft BOS (installation, contingency, engineering, land cost, and other soft BOS) and perovskite modules. Among electrocatalyst parts, the membrane is the crucial economic parameter and the replacement of the electrocatalyst also takes up a significant portion (57.4%) of the cost. The calculated LCOH is still relatively high compared to other hydrogen production processes such as natural gas reforming without carbon capture (0.5–1.7\$/kg<sup>40</sup>) and coal gasification (0.9–1.46\$/kg in China<sup>41</sup>). However, it could be cost-competitive compared to grid-connected water electrolysis (8.81\$/kg in the US<sup>42</sup>). It is also compared with other solar-to-hydrogen production methods, however, the range of the reported costs for hydrogen production is broad due to different technical and economic parameters. A thorough economic comparison is provided in Supplementary Information.

In addition to the base case, a sensitivity analysis is carried out to identify the parameters that have significant impacts on LCOH with several parameters in Supplementary Table 6. As a result of the parametric sensitivity analysis in Fig. 4c, the most critical parameter turns out to be  $\eta_{STH}$  followed by the capacity factor (i.e., availability of solar energy), discount rate, and module life span. The results from the sensitivity analysis are in line with the previous work<sup>43</sup>. Along with the maximum theoretical  $\eta_{STH}$  efficiency, ~20.5% cost reduction from the base case LCOH can be achieved while LCOH can be as high as 11.3\$/kg. Note that the capacity factor corresponds to the regional variations in solar energy and discount rate, the third impactful parameter, which is variable depending on a target system and those who conduct economic analysis. Therefore, the main systematic characteristics ( $\eta_{STH}$  and life span) are further investigated to quantify their impacts in terms of the economy with a broader range. As presented in Fig. 4d, a rapid cost reduction is observed as  $\eta_{STH}$  increases. When  $\eta_{STH}$  becomes

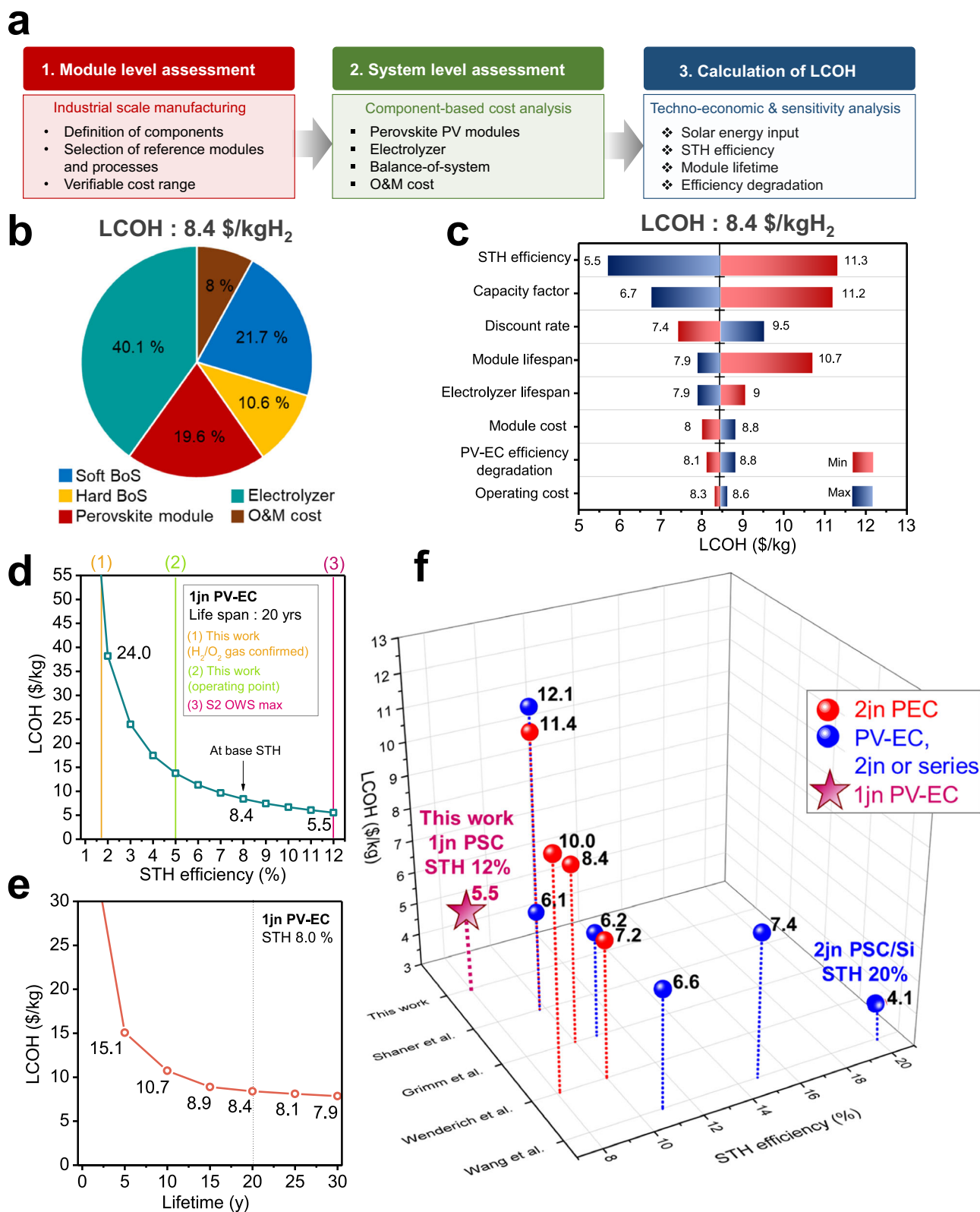


**Fig. 4 | Overview of techno-economic analysis (TEA) in this study. a** The flow chart of TEA, **b** cost breakdown of Levelized cost of hydrogen (LCOH), **c** the result of sensitivity analysis with several technical and economic parameters, and estimated LCOH depending on **d** solar-to-hydrogen efficiency acquired in this

manuscript (STH of 1.7% for gas evolution, 5.0% for operating point reading) and maximum STH for S2 OWS (12%) with assumption of life span of 20 years, and **e** the life span of the module with assumption that STH of 8.0%. **f** The result of economic performance comparison in terms of LCOH and  $\eta_{\text{STH}}$  from refs. [52,45,44,11](#).

double (6%) and three-fold (9%) from 3%, a cost reduction of 12.6 and 16.5\$/kg is acquired, respectively. In addition, an LCOH of 5.5\$/kg can be accomplished at the theoretically maximum  $\eta_{\text{STH}}$  (~12%). Similarly, the maximum life span can reduce the base LCOH to 7.9\$/kg corresponding to a cost reduction of 26.8% and 6.4% compared to the life span of 10 years and 20 years, respectively (Fig. 4e). In conclusion, the result indicates the room for improvement in terms of economic performance is greater for how efficiently the system converts solar energy to hydrogen, although both technical parameters are crucial for competitive environmentally favorable hydrogen production.

To validate hydrogen production cost using the S2 system proposed in this work, LCOH in the previous research works is compared with the TEA result. As presented in Fig. 4f, the higher the  $\eta_{\text{STH}}$ , the lower LCOH is observed in general. In addition, one of the promising solar energy-based hydrogen production technologies, photovoltaic connected to water electrolyzer, shows lower LCOH compared to hydrogen production using a PEC system because of the affordable cost of commercial Si-based photovoltaic and electrolyzer stack that has been continuously decreasing. Since LCOH is calculated through TEA with several different technical and economic parameters, an apple-to-apple comparison is not practically feasible so the parameters are presented in the Supplementary Table 9.

At a similar  $\eta_{\text{STH}}$  efficiency, the result of LCOH in this study (8.4\$/kg) is lower than the one reported in ref. 44 because the lower PV module price is assumed to reflect the benefit of single junction PV while dual light absorber is assumed in ref. 44 and others are similar in terms of cost. Compared to another work<sup>45</sup>, the results of calculated LCOH are the same (8.4\$/kg with  $\eta_{\text{STH}}$  8.0% in the base case, 5.5\$/kg with  $\eta_{\text{STH}}$  12.0% in the best case) although the PEC module price in the reference (153.71\$/m<sup>2</sup>) seems much greater than PV-EC in this study (40.0\$/m<sup>2</sup>). This is because the PEC module cost of 153.71\$/m<sup>2</sup> includes electrocatalysts, membrane, and wiring. The corresponding value in this study is 133.98\$/m<sup>2</sup> which is not much lower and the result seems reasonable.

## Discussion

We demonstrated a single junction PV-EC with CsPbBr<sub>3</sub> ( $E_g$  ~2.3 eV) solar cell, which achieved a  $V_{\text{OC}}$  larger than 1600 mV enough voltage for electrochemical overall water splitting. Currently achieved efficiency are ~3.4–3.0% for NiFeO<sub>x</sub>-Pt and 2.4% for IrO<sub>x</sub>-Pt for alkaline electrolyzers. For H<sub>2</sub> and O<sub>2</sub> gas evolution confirmed, STH of 1.7% was achieved from this work. Even though overall  $\eta_{\text{STH}}$  is very low compared to multi-junction or parallel connected PV-EC systems, our work presents an interesting perspective for the scenario of solar overall water splitting that requires only 1jn photovoltaic cell. TEA and expectation of theoretically achievable  $\eta_{\text{STH}}$  of ~12% showed its promising future to have LCOH of 5.5\$/kg, which would be commercialize if efficiency and stability of CsPbBr<sub>3</sub> PV is improved, which should happen in near future considering good progress made for wide band gap perovskite solar cell using CsPbBr<sub>3</sub> or MAPbBr<sub>3</sub> PV cells that PCE exceeding 11% were presented by group.

## Methods

### Materials for n-i-p CsPbBr<sub>3</sub> solar cells

Rubidium bromide (RbBr, 99.6%), cesium bromide (CsBr, 99.999%), lithium carbonate (Li<sub>2</sub>CO<sub>3</sub>, 99.99%), sodium carbonate (Na<sub>2</sub>CO<sub>3</sub>, 99.999%), potassium carbonate (K<sub>2</sub>CO<sub>3</sub>, 99.99%), rubidium carbonate (Rb<sub>2</sub>CO<sub>3</sub>, 99.8%), cesium carbonate (Cs<sub>2</sub>CO<sub>3</sub>, 99.9%), titanium diisopropoxide bis(acetylacetonate) (75 wt% in isopropanol), lead chloride (PbCl<sub>2</sub>, 99.999%), methanol (anhydrous, 99.8%), *N,N*-dimethylformamide (DMF, anhydrous, 99.8%), dimethyl sulfoxide (DMSO, anhydrous, ≥99.9%) and toluene (anhydrous, 99.8%) were purchased from Sigma-Aldrich. Lead bromide (PbBr<sub>2</sub>, >98.0%) was purchased from the Tokyo Chemical Industry. Methylammonium bromide (MABr, >99.99%) was purchased from Greatcell Solar. Colloidal tin(IV) oxide (SnO<sub>2</sub> colloidal

dispersion, 15% in H<sub>2</sub>O) was purchased from Alfa Aesar. Poly[bis(4-phenyl)(2,4,6-trimethylphenyl)amine] (PTAA) and F4-TCNQ were purchased from Jilin OLED. Molybdenum(VI) oxide (MoO<sub>3</sub>, ≥99.5%) was purchased from Daejung Chemicals & Metals.

### Fabrication of solar cells

Fluorine-doped tin oxide (FTO) glasses (TEC7, Pilkington) were cleaned with deionized water, acetone, and isopropyl alcohol sequentially by an ultrasonic cleaner. For the compact TiO<sub>2</sub> layer, the FTO glasses were placed on a hot plate and heated to 450 °C. The c-TiO<sub>2</sub> layer was deposited by spray pyrolysis method with 20 mL of a titanium diisopropoxide bis(acetylacetonate)/ethanol (1:10 v/v) solution. After the spray pyrolysis, the hot plate with the substrates was maintained at 450 °C for 1 h and then cooled down to room temperature. The prepared c-TiO<sub>2</sub> substrates were cleaned by UV-O<sub>3</sub> treatment and the SnO<sub>2</sub> layer was deposited by spin-coating at 3000 rpm with SnO<sub>2</sub> colloidal dispersion diluted to 1.70 wt%. The SnO<sub>2</sub>-coated substrates were annealed at 150 °C for 20 min. The Li<sub>2</sub>CO<sub>3</sub> solution was prepared by dissolving 5.17 mg of Li<sub>2</sub>CO<sub>3</sub> in 1 mL of deionized water. The Li<sub>2</sub>CO<sub>3</sub> solution was spin-coated on the SnO<sub>2</sub> surface at 3000 rpm and annealed at 300 °C for 5 min. After annealing, UV-O<sub>3</sub> treatment was performed on the Li<sub>2</sub>CO<sub>3</sub>-coated surface. For the deposition of the CsPbBr<sub>3</sub> perovskite layer, a multi-step deposition method was used. BX<sub>2</sub> solution with 1.0 mmol PbBr<sub>2</sub> and 0.09 mmol RbBr in 1 mL DMF/DMSO (9:1 v/v) mixture and AX solution with 0.07 mmol CsBr in 1 mL methanol were prepared. Prior to depositing a complete perovskite layer, the BX<sub>2</sub> solution was spin-coated at 2000 rpm and annealed at 90 °C for 20 min. Then, the AX solution was spin-coated 7 times, and each time was followed by annealing at 300 °C for 5 min. After the deposition of perovskite film, all substrates were transferred into an N<sub>2</sub>-filled glove box. 15 mg/mL of PTAA with 1 wt% of F4TCNQ in toluene solution was spin-coated on a perovskite layer and annealed at 100 °C for 10 min. Finally, MoO<sub>3</sub> (5 nm) and Au (60 nm) were sequentially deposited by thermal evaporation.

### Characterization of solar cells

The current density–voltage (*J*–*V*) characterizations of the devices were measured by a Keithley 2635A Source Measure Unit under AM 1.5 G with an intensity of 100 mW cm<sup>−2</sup> in an N<sub>2</sub>-filled glove box. The area of the device was 0.135 cm<sup>2</sup>. PV measurement QE system was used to measure incident photon to current efficiency (IPCE) under ambient conditions. A xenon arc lamp was used as the source of monochromatic light. Transient photovoltage (TPV) and transient photocurrent (TPC) measurements were conducted using McScience T4000 at open-circuit conditions and short-circuit conditions, respectively, under 1 sun illumination. Photoluminescence measurement was performed by Cary Eclipse (Varian) with 350 nm of excitation source. For the in-water stability measurement, the devices were encapsulated by glass sealed with epoxy resin and then soaked into a beaker filled with water.

### Perovskite film characterization

The CsPbBr<sub>3</sub> perovskite films were fabricated on the top of glasses by the multi-step deposition method as mentioned in “Device fabrication” section. Scanning electron microscope (SEM) images of perovskite solar cells were obtained by using a Hitachi High-Technology S-4800. The X-ray diffraction (XRD) pattern was characterized by using a Bruker D8 Advance diffractometer with Cu K $\alpha$  radiation ( $\lambda$  = 0.1542 nm) as the X-ray source. UV–visible absorption spectrum was taken by using a Varian Cary 5000 spectrophotometer. Ultraviolet photoelectron spectroscopy (UPS) was performed using ESCALAB 250XI equipment.

**Preparation of substrates.** FTO, Ti foil, Ni foil, and Ni foam were used as substrates for electrocatalysts in this work. FTO (TEC7, Pilkington)



was used after cleaning it with Helmanex soap water, DI water, Acetone, and Ethanol. For Ti foil (99.99%, Sigma Aldrich), was etched with 1 M oxalic acid (99.0%, Sigma Aldrich) for 1 h, 80 °C as the following protocol for removing surface oxide<sup>35</sup>. For Ni foil (99.98%, Sigma Aldrich) and Ni foam (99.5%, Invisible Inc.), the metal substrate was dipped in 0.1 M HCl (Samchun, 1.0 M of HCl 99.5% and diluted to 0.1 M) for 30 min prior to usage. Unless it is noted, the default size of the metal substrate was 1.0 cm × 1.0 cm.

**Fabrication of IrO<sub>x</sub>/Ti film.** IrO<sub>x</sub> was deposited on Ti foil, method was based on literature<sup>46</sup>. Sodium hexachloroiridate hexahydrate (Cl<sub>6</sub>IrNa<sub>2</sub>·6H<sub>2</sub>O, 99.9%, Sigma Aldrich) was used as received. 27 mg of the precursor was dissolved in acetyl acetone (>99.5%, Kanto chemical) (10 ml). 10 μl of the precursor solution was dropped on as prepared Ti foil with the size of 1.0 cm × 1.0 cm and dried in an ambient atmosphere, and finally put into 80 °C oven for full dryness. After 10 min, coated Ti foil was calcined at 500 °C for 20 min.

**Fabrication of Pt/Ti film.** Platinum(II) acetylacetonate (Pt(C<sub>5</sub>H<sub>7</sub>O<sub>2</sub>)<sub>2</sub>, 97.0%, Sigma Aldrich) was used as received. 57 mg of the precursor was dissolved in acetylacetone (15 ml). 10 μl of the precursor solution was dropped on as prepared Ti foil with the size of 1.0 cm × 1.0 cm and dried in an ambient atmosphere, and finally put into an 80 °C oven for full dryness. After 10 min, coated Ti foil was calcined at 500 °C for 20 min.

**Fabrication of Pt/Ni foil and foam.** Pt was deposited on the Ni foam or Ni foil by spontaneous galvanic displacement<sup>47</sup> with a small modification. 100 μL of H<sub>2</sub>PtCl<sub>6</sub> (8 wt% in DI water, Sigma Aldrich, 8 wt%) was added into 45 ml of 0.01 M HCl solution (Samchun, 1.0 M of HCl 99.5% and diluted to 0.01 M). And as prepared Ni foil or foam was dipped into the solution with mild stirring. The surface of Ni metal became black as an indicator of the Galvanic exchange of Ni/Pt (2Ni(s) + Pt<sup>4+</sup> → Pt(s) + 2Ni<sup>2+</sup>). After the dipping process, the substrate was taken out and washed with DI water, and ethanol in sequent.

**Fabrication of NiFeO<sub>x</sub>/Ni foil or Ni foam.** NiFe oxyhydroxide (or shortly noted as NiFeO<sub>x</sub>) was deposited by using anodic oxidation of cation in bicarbonate electrolyte with some modifications<sup>48</sup>. For solution, 40 mg of FeSO<sub>4</sub>·7H<sub>2</sub>O (≥99%; Sigma Aldrich) and 40 mg of NiSO<sub>4</sub>·6H<sub>2</sub>O (99%; Sigma Aldrich) were put in a glass bottle and 200 ml of 0.5 M KHCO<sub>3</sub> (99.7%, Sigma Aldrich) (pH of 8.3) was put in, resulting in a transparent and yellow solution. The existence of bicarbonate anion deters premature oxidation of Fe<sup>2+</sup> ion to iron hydroxide precipitation (which looks like orange-colored dust-like particles). For deposition, *I/V* curve with a bias range of 1.0–1.6 V vs. Ag/AgCl (without pretreatment) was applied (observed current range: 1–5 mA per 1.0 cm<sup>2</sup>) 20 times, with 100 mV/s scan rate. After repeating *I/V* curve, the surface of Ni metal becomes a slight orange-dark color.

**Preparation of CsPbBr<sub>3</sub>-IrO<sub>x</sub>/Pt artificial leaf.** FTO was used instead of Ti foil for making anodic and cathodic parts connected to the CsPbBr<sub>3</sub> cell. The aforementioned CsPbBr<sub>3</sub> solar cell with 4 × 0.135 = 0.54 cm<sup>2</sup> was connected to an anode and cathode with a geometric area of 0.25 cm<sup>2</sup>. After a conductive connection was made for both parts, epoxy was applied to prevent the electrolyte from getting into the solar cell.

**Characterization of the electrodes.** XRD was measured using PW3040/60 X'pert PRO, PANalytical with Cu Kα (0.154045 nm) radiation at 40 kV and 30 mA. High-resolution scanning electron microscopy (HRSEM, Hitach, SU-8220), and scanning transmission electron microscopy (STEM, JEOL, JEM-2100F) were analyzed to observe the morphology and interface of the materials. Energy dispersive X-ray spectroscopy (EDS) was conducted to confirm the atom composition.

Focused ion beam (Helios 450HP FIB, operated at 30 kV) cutting was conducted to see a cross-sectional inner view by STEM and EDS analysis. Ultraviolet–visible absorbance was measured with a UV–vis spectrometer (UV-2401 PC, Shimadzu). For X-ray (XPS) and UV photoelectron spectroscopy (UPS) (Thermo Fisher), a monochromatic Al Kα X-ray source was used.

**Electrochemical measurements.** Electrochemical and photovoltaic cell-assisted electrochemical cell analysis was conducted using two different modes—three-electrode cell Ag/AgCl (3.0 M NaCl) (BASI, MF-2052) and a Pt mesh wire as reference and counter electrodes, and two electrode cell with a specific configuration, respectively. Potentiostat (Ivium Technologies, A08013) was used for the measurement of three and two-electrode systems. An electrolyte of 1.0 M KOH (Samchun, 99.5%, pH 13.6) was used unless it was specified individually. For the light source, simulated 1 sun illumination (100 mW cm<sup>-2</sup>) generated by a solar simulator (Oriel, Newport 91160) with an AM 1.5 G filter. All potentials vs. the Ag/AgCl reference electrode were converted to the reversible hydrogen electrode (RHE) scale using the Nernst equation;

$$E_{RHE} = E_{Ag/AgCl} + 0.059 pH + E_{Ag/AgCl}^{\circ}$$

where  $E_{Ag/AgCl}$  is the experimental potential vs. Ag/AgCl reference electrode, and  $E_{Ag/AgCl}^{\circ}$  is 0.1976 V at 25 °C. Ag/AgCl reference electrode against Hg/HgO reference electrode (1.0 M NaOH) (ALS, RE-61AP) and measurement with Pt metal as Hydrogen evolution reaction, the value for  $E(Ag/AgCl)^{\circ}$  was near 0.1976 V and Hg/HgO was near 0.118 V as described in product catalogs (Supplementary Fig. 33). Measurement of PV-EC system is conducted with the same way as electrocatalysts but with simulated 1 sun illumination, the configuration is depicted in (Supplementary Fig. 34). All of *I/V* curves for (photo) electrochemical cell presented in this work is not *iR* corrected.

Incident photon to electron conversion efficiency (IPCE) for PV-EC system was measured with an Xe lamp as a light source (Oriel, Newport 6690S, 300 W) and a monochromator (Oriel, Newport 74004) operating in the wavelength range from 300 to 650 nm controlled by a power meter (Oriel, Newport 1936-R). Band width of the photon wavelength provided was 10 nm. Current generated from PV-EC was measured under 0.0 V versus counter electrode and converted into current density by using the active area of PV with mask and converted to IPCE by the following formula:

$$IPCE = \frac{1240 \times J (mA cm^{-2})}{P_{light} (mW cm^{-2}) \times \lambda (nm)}$$

where  $J$  is the measured photocurrent density using a monochromator,  $P_{light}$  is the calibrated illumination power of specific wavelength and  $\lambda$  is the wavelength of the incident light.

**On-line gas product analysis.** Gas evolution experiment was conducted using a custom gas-tight electrochemical cell reactor (50 mL volume, 30 mL electrolyte + 20 mL head space) without a membrane. The reactor was purged with high purity Ar gas (99.999%, institute supply from UNIST) for 60 min prior to application of potential. Gas generated under applied potential was quantified by a gas chromatograph (Agilent, GC 6890) with a packed column (Supelco, Carboxen 1000) and a thermal conductivity detector (TCD). High-purity Ar gas (99.999%, institute supply from UNIST) was used as a carrier gas, and the cell was analyzed with an Ar flow rate of 10 sccm.

**Estimation of Levelized cost of hydrogen.** To evaluate the economic performance of the system for solar energy-based hydrogen production, the Levelized cost of hydrogen (LCOH) is estimated based on techno-economic analysis (TEA). As shown in Fig. 4a, the LCOH of the system is estimated based on the three-step costing strategy: (1)



module level, (2) system level, and (3) parametric sensitivity analysis. In the first step, the cost range of the single junction perovskite solar cell proposed in this study is verified based on previously reported works. In the system-level estimation, components for the system are identified first. The components for one-step solar-based hydrogen production utilizing the proposed system are perovskite modules, electrocatalysts, and balance-of-system (BOS) such as structural materials, wiring, water, and gas processing units. Besides the capital expenditure, operation and maintenance (O&M) costs including labor costs and an alkaline solution are also considered. The detailed normalized costs (\$/m<sup>2</sup>) of each system component are provided in Supplementary Table 6. Confirming overall components and system cost, the LCOH of the system is calculated based on the equation

$$\text{LCOH} (\$/\text{kg}) = \frac{\sum_{t=1}^n \frac{(\text{Invest}_t + \text{OnM}_t)}{(1+r)^t}}{\sum_{t=1}^n \frac{P_t}{(1+r)^t}}$$

where Invest<sub>*t*</sub> is the initial investment (\$) in year *t*, OnM<sub>*t*</sub> is the operation and maintenance expenditure (\$) in year *t*, *P<sub>t</sub>* is the annual production of hydrogen (kg/yr) in year *t*, *r* is the discount rate in %, and *n* is the life span of the system. Techno-economic parameters applied in this study are presented in Supplementary Table 5.

## Data availability

All the relevant data are available from the corresponding authors upon reasonable request. Source data are provided with this paper.

## References

- Lewis, N. S. Research opportunities to advance solar energy utilization. *Science* **351**, aad1920 (2016).
- Seh, Z. W. et al. Combining theory and experiment in electrocatalysis: Insights into materials design. *Science* **355**, eaad4998 (2017).
- Davis, S. J. et al. Net-zero emissions energy systems. *Science* **360**, eaas9793 (2018).
- Wei, C. et al. Recommended practices and benchmark activity for hydrogen and oxygen electrocatalysis in water splitting and fuel cells. *Adv. Mater.* **31**, 1806296 (2019).
- Pinaud, B. A. et al. Technical and economic feasibility of centralized facilities for solar hydrogen production via photocatalysis and photoelectrochemistry. *Energy Environ. Sci.* **6**, 1983–2002 (2013).
- Takata, T. et al. Photocatalytic water splitting with a quantum efficiency of almost unity. *Nature* **581**, 411–414 (2020).
- Wang, Q. et al. Scalable water splitting on particulate photocatalyst sheets with a solar-to-hydrogen energy conversion efficiency exceeding 1%. *Nat. Mater.* **15**, 611–615 (2016).
- Qiu, Y. et al. Efficient solar-driven water splitting by nanocone BiVO<sub>4</sub>-perovskite tandem cells. *Sci. Adv.* **2**, e1501764 (2016).
- Cheng, W.-H. et al. Monolithic photoelectrochemical device for direct water splitting with 19% efficiency. *ACS Energy Lett.* **3**, 1795–1800 (2018).
- Jia, J. et al. Solar water splitting by photovoltaic-electrolysis with a solar-to-hydrogen efficiency over 30. *Nat. Commun.* **7**, 13237 (2016).
- Wang, Y. et al. Direct solar hydrogen generation at 20% efficiency using low-cost materials. *Adv. Energy Mater.* **11**, 2101053 (2021).
- Abbasi, R. et al. A roadmap to low-cost hydrogen with hydroxide exchange membrane electrolyzers. *Adv. Mater.* **31**, 1805876 (2019).
- Kibsgaard, J. & Chorkendorff, I. Considerations for the scaling-up of water splitting catalysts. *Nat. Energy* **4**, 430–433 (2019).
- Chang, W. J. et al. Design principle and loss engineering for photovoltaic-electrolysis cell system. *ACS Omega* **2**, 1009–1018 (2017).
- Kim, J. H., Kim, Y. K. & Lee, J. S. Perovskite tandems advance solar hydrogen production. *Joule* **3**, 2892–2894 (2019).
- Sayama, K. & Miseki, Y. Research and development of solar hydrogen production. *Synthesiol. Engl. Ed.* **7**, 79–91 (2014).
- Sayama, K. Production of high-value-added chemicals on oxide semiconductor photoanodes under visible light for solar chemical-conversion processes. *ACS Energy Lett.* **3**, 1093–1101 (2018).
- Miseki, Y. & Sayama, K. Photocatalytic water splitting for solar hydrogen production using the carbonate effect and the Z-scheme reaction. *Adv. Energy Mater.* **9**, 1801294 (2019).
- Sathre, R. et al. Opportunities to improve the net energy performance of photoelectrochemical water-splitting technology. *Energy Environ. Sci.* **9**, 803–819 (2016).
- Ardo, S. et al. Pathways to electrochemical solar-hydrogen technologies. *Energy Environ. Sci.* **11**, 2768–2783 (2018).
- Kim, J. H., Hansora, D., Sharma, P., Jang, J.-W. & Lee, J. S. Toward practical solar hydrogen production – an artificial photosynthetic leaf-to-farm challenge. *Chem. Soc. Rev.* **48**, 1908–1971 (2019).
- Vilanova, A., Dias, P., Lopes, T. & Mendes, A. The route for commercial photoelectrochemical water splitting: a review of large-area devices and key upscaling challenges. *Chem. Soc. Rev.* **53**, 2388–2434 (2024).
- Wang, Y. et al. A single-junction cathodic approach for stable unassisted solar water splitting. *Joule* **3**, 2444–2456 (2019).
- Liu, S. et al. Buried interface molecular hybrid for inverted perovskite solar cells. *Nature* **632**, 536–542 (2024).
- Luo, J. et al. Water photolysis at 12.3% efficiency via perovskite photovoltaics and Earth-abundant catalysts. *Science* **345**, 1593–1596 (2014).
- Gao, J. et al. Solar water splitting with perovskite/silicon tandem cell and TiC-supported Pt nanocluster electrocatalyst. *Joule* **3**, 2930–2941 (2019).
- Sun, Q. et al. Integrated 4-terminal all-inorganic perovskite tandem solar cell with open-circuit voltage exceeding 2.1 V for water splitting. *ACS Energy Lett.* **7**, 4215–4223 (2022).
- Rühle, S. Tabulated values of the Shockley–Queisser limit for single junction solar cells. *Sol. Energy* **130**, 139–147 (2016).
- Tao, S. et al. Absolute energy level positions in tin- and lead-based halide perovskites. *Nat. Commun.* **10**, 2560 (2019).
- He, R. et al. Wide-bandgap organic–inorganic hybrid and all-inorganic perovskite solar cells and their application in all-perovskite tandem solar cells. *Energy Environ. Sci.* **14**, 5723–5759 (2021).
- Kulbak, M. et al. Cesium enhances long-term stability of lead bromide perovskite-based solar cells. *J. Phys. Chem. Lett.* **7**, 167–172 (2016).
- Tran, V.-H., Park, H., Eom, S. H., Yoon, S. C. & Lee, S.-H. Modified SnO<sub>2</sub> with alkali carbonates as robust electron-transport layers for inverted organic solar cells. *ACS Omega* **3**, 18398–18410 (2018).
- Jeong, J. et al. Formamidineium-based planar heterojunction perovskite solar cells with alkali carbonate-doped zinc oxide layer. *RSC Adv.* **8**, 24110–24115 (2018).
- Kim, J. H. et al. Wireless solar water splitting device with robust cobalt-catalyzed, dual-doped BiVO<sub>4</sub> photoanode and perovskite solar cell in tandem: a dual absorber artificial leaf. *ACS Nano* **9**, 11820–11829 (2015).
- Fehr, A. M. K. et al. Integrated halide perovskite photoelectrochemical cells with solar-driven water-splitting efficiency of 20.8%. *Nat. Commun.* **14**, 3797 (2023).
- Duan, J., Zhao, Y., Wang, Y., Yang, X. & Tang, Q. Hole-boosted Cu(Cr,M)O<sub>2</sub> nanocrystals for all-inorganic CsPbBr<sub>3</sub> perovskite solar cells. *Angew. Chem. Int. Ed.* **58**, 16147–16151 (2019).
- Fontaine, K. T., Lewerenz, H. J. & Atwater, H. A. Efficiency limits for photoelectrochemical water-splitting. *Nat. Commun.* **7**, 13706 (2016).

38. Seger, B. et al. 2-Photon tandem device for water splitting: comparing photocathode first versus photoanode first designs. *Energy Environ. Sci.* **7**, 2397–2413 (2014).
39. Fehr, A. M. K., Deutsch, T. G., Toma, F. M., Wong, M. S. & Mohite, A. D. Technoeconomic model and pathway to <\$2/kg green hydrogen using integrated halide perovskite photoelectrochemical cells. *ACS Energy Lett.* **8**, 4976–4983 (2023).
40. *Global Hydrogen Review 2021*, International Energy Agency, <https://www.iea.org/reports/global-hydrogen-review-2021> (2021).
41. Li, J., Wei, Y.-M., Liu, L., Li, X. & Yan, R. The carbon footprint and cost of coal-based hydrogen production with and without carbon capture and storage technology in China. *J. Clean. Prod.* **362**, 132514 (2022).
42. Christensen, A. *Assessment of Hydrogen Production Costs from Electrolysis: United States and Europe, 2025 International Council on Clean Transportation*, <https://theicct.org/publication/assessment-of-hydrogen-production-costs-from-electrolysis-united-states-and-europe/> (2020).
43. Yates, J. et al. Techno-economic analysis of hydrogen electrolysis from off-grid stand-alone photovoltaics incorporating uncertainty analysis. *Cell Rep. Phys. Sci.* **1**, 100209 (2020).
44. Wenderich, K. et al. Industrial feasibility of anodic hydrogen peroxide production through photoelectrochemical water splitting: a techno-economic analysis. *Sustain. Energy Fuels* **4**, 3143–3156 (2020).
45. Grimm, A., de Jong, W. A. & Kramer, G. J. Renewable hydrogen production: a techno-economic comparison of photoelectrochemical cells and photovoltaic-electrolysis. *Int. J. Hydrog. Energy* **45**, 22545–22555 (2020).
46. Pan, L. et al. Cu<sub>2</sub>O photocathodes with band-tail states assisted hole transport for standalone solar water splitting. *Nat. Commun.* **11**, 318 (2020).
47. Milazzo, R. G., Privitera, S. M. S., Scalese, S. & Lombardo, S. A. Effect of morphology and mechanical stability of nanometric platinum layer on nickel foam for hydrogen evolution reaction. *Energies* **12**, 3116 (2019).
48. Kim, J. H. et al. Seawater-mediated solar-to-sodium conversion by bismuth vanadate photoanode- photovoltaic tandem cell: solar rechargeable seawater battery. *iScience* **19**, 232–243 (2019).
49. Liu, J. et al. Metal-free efficient photocatalyst for stable visible water splitting via a two-electron pathway. *Science* **347**, 970–974 (2015).
50. Wang, Z. et al. Overall water splitting by Ta<sub>3</sub>N<sub>5</sub> nanorod single crystals grown on the edges of KTaO<sub>3</sub> particles. *Nat. Catal.* **1**, 756–763 (2018).
51. Wang, Q. et al. Oxy sulfide photocatalyst for visible-light-driven overall water splitting. *Nat. Mater.* **18**, 827–832 (2019).
52. Shaner, M. R., Atwater, H. A., Lewis, N. S. & McFarland, E. W. A comparative technoeconomic analysis of renewable hydrogen production using solar energy. *Energy Environ. Sci.* **9**, 2354–2371 (2016).

## Acknowledgements

This work was supported by the Climate Change Response Project (NRF-2019M1A2A2065612), and Brainlink Project (NRF-2022H1D3A3A0108 1140) funded by the Ministry of Science and ICT of Korea via the National Research Foundation. J.H. Kim gratefully acknowledges the support

from the Basic Science Research Program funded by the Ministry of Education (NRF-2021R1A6A3A14039651, NRF-2019R1A6A3A01096197). This work was supported by the National Research Foundation of Korea (NRF) grant funded by the Korean government (MSIT) (RS-20240034 6361) and the Carbon Neutrality Demonstration and Research Center of UNIST (Ulsan National Institute of Science and Technology).

## Author contributions

J.H.K. and J.Y.K. conceived and designed the project. J.S., J.L., H.L., and J.K. fabricated and characterized lead bromide perovskite solar cells. D.L. and J.A.M. conducted techno-economical analysis. J.H.K. and J.U.L. fabricated and characterized the electrocatalysts and conducted analysis for solar overall water splitting. J.H.K., M.G., H.L., J.S.L., and J.Y.K. supervised the project. J.J., S.M.Z., and S.C. helped edit and review the manuscript. J.H.K., J.S., and D.L., H.L., J.S.L., and J.Y.K. co-wrote and participated in editing and reviewing the manuscript.

## Competing interests

The authors declare no competing interests.

## Additional information

**Supplementary information** The online version contains supplementary material available at <https://doi.org/10.1038/s41467-025-58980-3>.

**Correspondence** and requests for materials should be addressed to Jin Hyun Kim, Hankwon Lim, Jae Sung Lee or Jin Young Kim.

**Peer review information** *Nature Communications* thanks Kun Chang, Jingshan Luo and the other anonymous reviewer(s) for their contribution to the peer review of this work. A peer review file is available.

**Reprints and permissions information** is available at <http://www.nature.com/reprints>

**Publisher's note** Springer Nature remains neutral with regard to jurisdictional claims in published maps and institutional affiliations.

**Open Access** This article is licensed under a Creative Commons Attribution-NonCommercial-NoDerivatives 4.0 International License, which permits any non-commercial use, sharing, distribution and reproduction in any medium or format, as long as you give appropriate credit to the original author(s) and the source, provide a link to the Creative Commons licence, and indicate if you modified the licensed material. You do not have permission under this licence to share adapted material derived from this article or parts of it. The images or other third party material in this article are included in the article's Creative Commons licence, unless indicated otherwise in a credit line to the material. If material is not included in the article's Creative Commons licence and your intended use is not permitted by statutory regulation or exceeds the permitted use, you will need to obtain permission directly from the copyright holder. To view a copy of this licence, visit <http://creativecommons.org/licenses/by-nc-nd/4.0/>.

© The Author(s) 2025